Review Article Vol. 6, No. 4 / April 2019 / Optica 479

Light-scattering methods for tissue diagnosis

Zachary A. Steelman,* Derek S. Ho, Kengyeh K. Chu, and Adam Wax

Department of Biomedical Engineering, Duke University, 101 Science Dr., Durham, North Carolina 27705, USA
**Corresponding author: zachary.steelman@duke.edu*

Received 11 February 2019; revised 14 March 2019; accepted 14 March 2019 (Doc. ID 359862); published 12 April 2019

Light scattering has become a common biomedical research tool, enabling diagnostic sensitivity to myriad tissue alterations associated with disease. Light–tissue interactions are particularly attractive for diagnostics due to the variety of contrast mechanisms that can be used, including spectral, angle-resolved, and Fourier-domain detection. Photonic diagnostic tools offer further benefits in that they are non-ionizing, non-invasive, and give real-time feedback. In this review, we summarize recent innovations in light-scattering technologies, with a focus on clinical achievements over the previous ten years.

https://doi.org/10.1364/OPTICA.6.000479

1. INTRODUCTION

The study of light–matter interactions has been a primary driver of scientific discovery for hundreds of years. From the earliest days of rationalizing the color of the night sky, to the wave-particle duality that captivated Newton and Huygens, to the detection of gravitational waves, light has proven to be a powerful tool for understanding our world. Although this interaction has primarily been restricted to studying fundamental physics, in the past twenty years, light scattering has become central to both established and emerging biomedical applications [1].

The theory of light scattering has a reputation for complexity, with massive volumes devoted to the study of scattering by objects of relatively simple geometry. Indeed, the classical "inverse problem" of light scattering—that of extracting complete knowledge of an object by measuring its scattered field—is terribly difficult [2,3]. Inverse scattering problems are ill conditioned, in that different combinations of object geometries, and of the optical indices of the object and medium, can produce a similar scattered field, and the difficulty is compounded by limitations of the measurement process. Theoretical frameworks of varying complexity help to reduce the degrees of freedom associated with the problem of uniqueness, while regularization and statistical methods can be used to diminish measurement errors.

Biomedical applications of light scattering are further complicated by the complexity of biological tissues. Unlike the dielectric sphere studied by Mie [4], tissues exhibit heterogeneity at nearly every length scale. Organization at some scales is countered by disorder at others, with unique distributions of material at the molecular, sub-cellular, cellular, and structural levels. While the intricacy of tissue certainly introduces difficulty for the inverse problem, it also signifies the wealth of information available for quantitative analysis.

Light-scattering diagnostic applications are attractive in part because of the wide array of parameters available for measurement. Information encoded in the wavelength [5], wavevector [6], polarization [7], and phase [8] of scattered light may be diagnostically relevant, while optical phenomena such as interference [9] and propagation [10] can reveal previously unmeasurable quantities. The richness of information in the scattered field has led to a wide array of technologies that measure one or more parameters to extract meaningful information from tissue.

In this review, we give an overview of the current state of biomedical applications of light scattering, with a focus on emerging tools over approximately the last ten years. Particular focus is given to applications in tissue, with occasional reference to *in vitro* studies that lay important groundwork for clinical techniques or that utilize similar contrast mechanisms to *in vivo* technologies to solve a clinical need. While the methods are highly varied and often overlap substantially, we have organized our analysis primarily by contrast mechanism. Sections covering wavelength-dependent scattering, angle-resolved scattering, and Fourier-domain methods are introduced. Optical instrumentation and data analysis are discussed for each technique, with particular focus on clinical results.

2. WAVELENGTH-DEPENDENT LIGHT SCATTERING

Like most optical processes, elastic scattering in tissue is characterized by a substantive dependence on the wavelength of incident light. A number of techniques have been developed that analyze the spectrum of scattered light from tissue for clinical diagnostic purposes. An overview of these techniques is given below, with a focus on recent developments.

A. Elastic-Scattering Spectroscopy and Light-Scattering Spectroscopy

Elastic scattering spectroscopy (ESS) is a non-invasive optical technique that analyzes the spectrum of diffuse scattering in tissue for clinical diagnostic purposes [11]. In typical implementations, light from a broadband source is coupled into a multimode fiber, the distal end of which is placed in direct contact with the tissue to be analyzed. A secondary fiber or fibers placed near the illumination

spot collect diffusely scattered photons, which are coupled into a spectrometer for data analysis. ESS has been demonstrated in clinical trials for diagnosis of breast cancer [12], colonic lesions [13], and high-grade dysplasia in Barrett's esophagus [14], among others.

Spectral analysis in ESS may take many forms and may include direct analysis of specific spectral regions [11], identification of diagnostically relevant portions of the spectrum with machine learning [15], or extraction of tissue optical properties (such as the reduced scattering coefficient, blood volume fraction, or hemoglobin oxygen saturation) by fitting the acquired spectrum to an appropriate model [16]. The best-suited method of analysis is chosen according to the desired application.

In recent years, ESS has expanded to include a wide array of potential applications. Suh *et al.* have suggested ESS for discriminating benign from malignant disease in *ex vivo* thyroid samples [17]. Rodriguez-Diaz *et al.* have conducted a more recent study of colonic polyps, finding >90% sensitivity and specificity for detecting neoplastic polyps [18]. Trials have also been completed showing the ability of ESS to distinguish malignant from benign skin lesions [19] as well as to distinguish between benign, dysplastic, and inflammatory prostate samples *ex vivo* [15].

It should be noted that ESS is sometimes labelled diffuse reflectance spectroscopy, a technique that is similar to ESS but that may encompass both contact and non-contact probes [20]. A vast literature exists on this topic, so we focus here on new developments. In recent years, diffuse reflectance spectroscopy has been applied to *in vivo* diagnosis of skin cancer [21] and combined with fluorescence measurements for breast surgical margin analysis [22] and identification of peripheral lung tumors [23].

A related technique to elastic scattering spectroscopy is light-scattering spectroscopy (LSS). Like ESS, LSS analyzes the spectrum of scattered light to determine the morphological properties of tissue. Unlike ESS, LSS seeks to extract light that has been singly scattered, which can then be analyzed using Mie theory [5] or more sophisticated models [24]. Analysis of spectral oscillations yields parameters like the size distributions of nuclei, their population density, and refractive index relative to the cytoplasm [25].

In traditional implementations of LSS, light from a broadband source is linearly polarized and directed onto the tissue or cell monolayer surface to be analyzed. Scattered light is passed through an analyzer to the detector plane in a manner sometimes referred to as polarization-gated LSS [26]. Spectral discrimination occurs by filtering the input light to a narrow, tunable spectral range or by using a spectrally selective means of detection such as a spectrometer or tunable filter. Typically, two measurements of the scattered light are taken, with the analyzer parallel and perpendicular to the illumination polarization axis, respectively. Subtraction of the depolarized component $I_{\perp}$ from the coplanar component $I_{\parallel}$ yields an intensity ΔI that attempts to isolate singly scattered photons from the upper epithelium, which have maintained their polarization state. Polarization subtraction is particularly useful in tissue, as it attempts to remove the contribution of the unpolarized diffusive background. ΔI is acquired for a number of wavelengths and may also be acquired for various scattering angles [27] or object locations in an imaging configuration [25]. Spectra may also be acquired using an optical fiber probe for *in vivo* applications [28]. The resulting spectrum is fitted to an analytical model based on Mie theory, with the best fits used to predict nuclear crowding and size distributions. The results correlate highly with those obtained by light microscopy and are a significant biomarker in histopathological dysplasia detection.

Recent work in LSS has focused on Barrett's esophagus and other endoscopic applications. Qiu *et al.* has demonstrated a scanning instrument capable of detecting dysplasia in Barrett's esophagus with 92% sensitivity and 96% specificity [29], and in a more recent study has demonstrated 96% and 97% sensitivity and specificity, respectively [30]. Patel *et al.* have used polarization-gated LSS of the duodenal mucosa to detect an early increase in blood supply (EIBS) associated with neoplastic lesions in the pancreas [31]. Further, Zhang *et al.* have verified the ability of LSS to identify the malignant potential of pancreatic cystic lesions during endoscopy [32]. Representative figures from this study are displayed in Fig. 1.

B. Diffuse Reflectance Modeling

The validity of spectral analysis of diffuse reflectance relies heavily on analytical models of varying complexity. One of the most common standards is based on a steady-state diffusion model of light scattering, which describes the radial dependence of diffuse reflectance from tissue [33]. In a seminal paper, Zonios *et al.* used the diffusion model to extract hemoglobin concentration, hemoglobin oxygen saturation, effective scatterer density, and effective scatterer size from diffuse reflectance measurements of normal and adenomatous colon *in vivo* [34], with adenomatous tissues showing a marked increase in hemoglobin concentration.

In recent years, diffuse reflectance modeling has been understudied compared with other methods. However, there have been a few advances of note. Improved computational schemes have enabled the use of Monte Carlo methods for arbitrary collection geometries, enabling semi-empirical approximations of diffuse reflectance to replace complex analytic solutions [35]. Two-layers models have been introduced, which more realistically model the vast majority of biological tissues that exhibit an epithelial layer [36]. Additionally, the influence of the phase function has been studied, demonstrating the importance of the probabilistic angular scattering distribution on model results [37]. The long-term trend towards parallelized, high-throughput computing could lead to a resurgence in this type of modeling.

C. Spectroscopic OCT

Optical coherence tomography (OCT) is a well-known biomedical imaging technique that creates tomographic images of tissues with a resolution on the order of a few micrometers. While traditional OCT creates depth-resolved reflectivity maps, functional information is not generally available. To solve this problem, spectroscopic OCT (SOCT) allows encoding of spectral information into the tomographic images. SOCT traditionally uses a windowing method [38], such as the short-time Fourier transform (STFT), in which spectral fringes are isolated from wavelength-specific regions to create a series of spectroscopically distinct tomograms. The properties of the window may be chosen according to the desired spectral resolution, which contains a well-known trade-off with depth resolution in the resulting image.

SOCT has become a popular tool for characterizing tissues, since only an additional processing step is required to obtain spectral information from a Fourier-domain OCT instrument. Here, we present some of the major developments in SOCT in recent years. To overcome the trade-off in depth versus spectral resolution, Robles *et al.* have introduced a dual-window (DW) method,

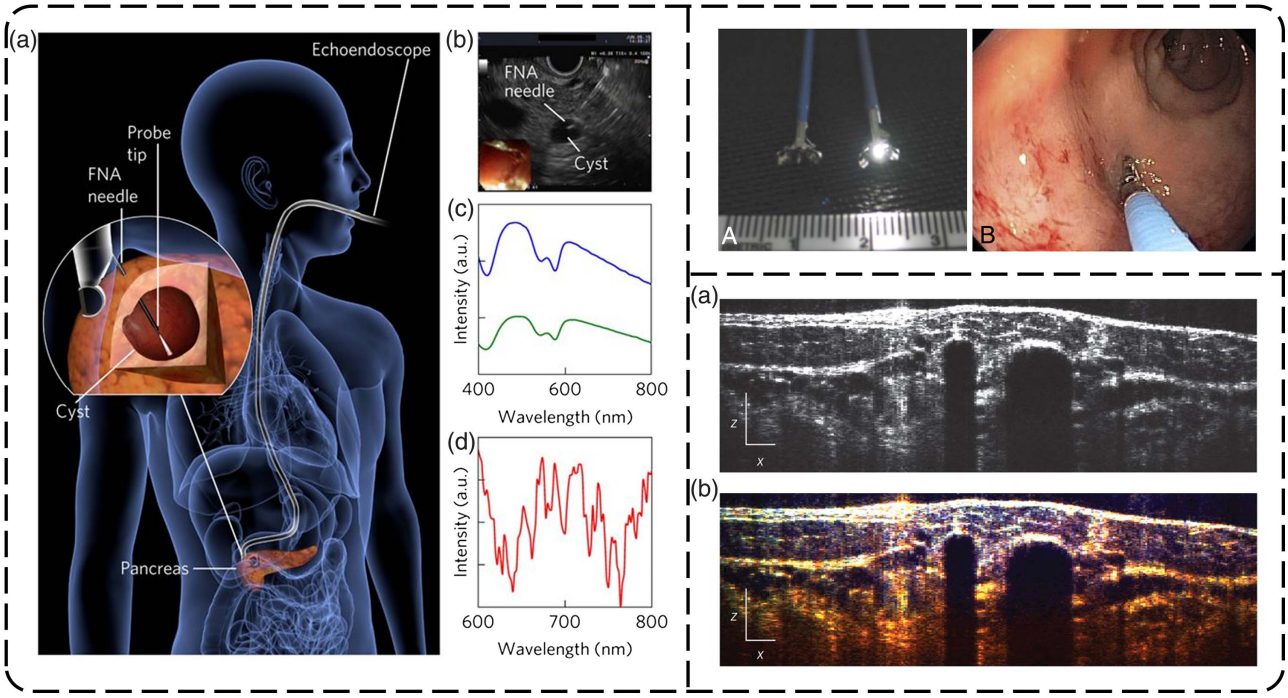

Fig. 1. (Left) (a) Illustration demonstrating an endoscopic ultrasound-guided fine-needle aspiration procedure for optical biopsy of the pancreas using LSS. (b) Endoscopic ultrasound image of the needle probe penetrating the cyst. (c) Spectra collected from two distinct source-detector separations and (d) backscattering component obtained from the LSS spectrum. (Top Right) (a) Comparison of standard biopsy forceps with integrated dual-fiber probe forceps for ESS and (b) use of forceps for polyp assessment using ESS. (Bottom Right) (a) Conventional OCT image and (b) molecular imaging true-color spectroscopic OCT, which uses a dual-window method for spectral analysis. Reproduced with permission Refs. [18,32,40]. 2015, Elsevier and 2017, 2011, Springer Nature.

which uses two spectral window functions of different bandwidths followed by a point-by-point multiplication to preserve depth resolution [39,40]. Yi *et al.* have developed a processing scheme referred to as inverse spectroscopic OCT (ISOCT), which measures wavelength-dependent scattering coefficients using a forward model and uses these parameters to deduce the refractive index correlation function in tissue [41]. ISOCT is useful for probing the ultrastructural nature of tissues and has been used to study field carcinogenesis in the pancreas and colon [42].

Clinical applications for SOCT continue to develop for several tissue types. Zhao *et al.* has shown the ability of SOCT to quantify burn severity in a mouse model [43]. Visible-light spectroscopic OCT has been suggested for a number of applications, including retinal oximetry [44], microvascular hemoglobin mapping [45], examination of amyloid beta plaques in the human and mouse brain [46], bilirubin quantification in tissue phantoms [47], and elastic light-scattering spectroscopy in the visible and near infrared [48]. Though applications in oncology have been more limited, Kassinopoulos *et al.* have demonstrated that a correlation of the spectral derivative from SOCT may be utilized to estimate scatterer size, with good performance distinguishing normal from cancerous human colon *ex vivo* [49]. Spectroscopic OCT remains a highly active research area.

D. Dark-Field Spectral Scatter Imaging

Spectroscopic analysis of resected tissue may be performed using more conventional microscopy configurations. One such technique is dark-field spectral scatter imaging, originally developed by Krishnaswamy *et al.* [50]. In this method, a broadband supercontinuum light source is collimated onto a dark-field aperture stop, creating a hollow cylindrical beam that is focused onto the sample. Orthogonal galvanometer-based scanning mirrors are used for raster scanning, while a custom, broadband f-theta scan lens ensures telecentricity. A CCD-based spectrometer is placed in the detection pathway. The result is a system that efficiently and quickly analyzes the spectral properties of scattered light while rejecting specular reflected photons.

Dark-field spectral scatter imaging has shown promise in the assessment of breast surgical margins. In particular, this approach achieved 93% sensitivity and 95% specificity in distinguishing benign from malignant pathologies using a threshold-based classifier [51]. Unique spectral signatures from distinct breast pathologies have also been identified, including fibrocystic disease, invasive breast carcinoma, and ductal carcinoma *in situ* [52].

E. Partial Wave Spectroscopy

Conventional light-scattering methods are typically focused on assessing structural changes at the wavelength scale or longer. However, recent work has shown that nanoscale sensitivity is also possible. The approach, termed partial wave spectroscopy (PWS) is based on analyzing spectral fluctuations of backscattered light to determine correlations within the sample [53]. Analysis of these correlations can then be used to assess the health status of individual cells [54].

The PWS approach became a significant optical diagnostic technique when it was linked to the field carcinogenesis effect [55]. In this interpretation, the conditions that may cause carcinogenesis to occur in one site in an organ should be prevalent at

other locations in that organ. For example, PWS studies showed that measurements of cytology brushings from histologically normal rectal mucosa can reveal the presence of cancer at distant sites in the colon [56]. The observed changes in PWS signals have also been linked to changes in subcellular features such as chromosome [57] and cytoskeleton [58] organization.

3. ANGLE-RESOLVED LIGHT SCATTERING

Tumorigenic cells exhibit a number of morphologic variations from healthy cells, including changes in the size and shape of the cell, nuclei, and cytoplasmic organelles and alterations in the nuclear-to-cytoplasmic ratio and chromatin structure. Because angular light scattering is highly sensitive to alterations in scatterer properties, angle-resolved scatter detection is a useful tool for the measurement of subcellular morphology. In many cases, angle-resolved light scattering has been used to predict the presence of early carcinogenesis. An overview of these techniques is given below.

A. Goniometric Measurements

Early studies of angular scattering used a goniometer system to measure the angle-resolved light-scattering intensity from suspended cells, isolated nuclei, and mitochondria to demonstrate that light scattering is sensitive to changes in the morphological structure of organelles [59,60]. In the goniometer system, a collimated beam of light is incident on a tank, which is filled with an index-matching solution and the sample located at the center of the rotation axis. A detector is rotated about the sample on the goniometer arm to collect and map the scattered light intensity as a function of angle. By fitting the angular scattering data to simulated scattering distributions of spherical and ellipsoidal scatterers, the size distribution of scatterers can be determined [61].

To better understand the light-scattering properties of tissue, goniometric measurements have been taken using multicellular spheroids, which better mimic the 3D micro-environment and organization of tumors *in vivo*. A comparison between intact and dissociated spheroids found general similarity in the angle-resolved light scattering, suggesting that cell–cell interactions, cell shape, and the intercellular matrix do not significantly contribute to angular light scattering in spheroids [62]. However, in the same study, tumorigenic spheroids showed higher relative backscatter intensity when compared to healthy spheroids, consistent with prior results suggesting that rapidly growing cells produce higher backscattering. Spectral, polarimetric, and angular light-scattering measurements were also performed on tumor spheroids, where light depolarization was found to be dependent on scattering angle [63]. This effect was attributed to multiple scattering events caused by internal cellular organelles.

Recently, a similar goniometric system was used to acquire angular light-scattering measurements from Hela cells in different phases of the cell cycle. It was demonstrated that the intensity of low-angle, forward-scattered light and high-angle, backscattered light can be linked to cell size and DNA content within the cell, respectively [64]. Further study of these optical signatures can provide relevant information on the physiologic structure of tumor cells.

B. Finite-Difference Time-Domain Methods

While analytic solutions of angular scattering exist for geometrically simple objects, cells and tissues exhibit substantial optical heterogeneity [67,68], making exact solutions of the angular scattering problem difficult. Finite-difference time-domain (FDTD) computational methods have been used to predict scattering distributions for cells and organelles of arbitrary shape and refractive index [60]. The FDTD algorithm spatially and temporally discretizes the Maxwell equations, which are solved over multiple time steps using finite-difference equations within a 3D lattice of grid points. Using FDTD, angular scattering was determined to be sensitive to changes between healthy and precancerous cells, particularly in regards to nuclear atypia [69,70]. Recent implementations of the FDTD algorithm have been greatly accelerated through GPU-based execution, enabling more complex light-scattering analysis [71–73]. Using these algorithms, various groups have explored the effects of nuclear size and refractive index [74,75], collagen fiber networks [76], and epithelial depth [77] on light scattering through neoplastic progression in cells.

C. Four-Dimensional Elastic Light-Scattering Fingerprinting

As this review notes, both spectral and angular scattering information are useful in extracting morphological information from cells. A technique for measuring both properties, termed four-dimensional elastic light-scattering fingerprinting (4D-ELF) was developed by Roy *et al.* An extension of light-scattering spectroscopy, 4D-ELF measures spectral, angular, azimuthal, and polarization dependence of light scattering from a sample and uses the angular scattering data to calculate higher fractal dimensions in tissue architecture during carcinogenesis [65,78]. A simplified endoscopic version of this technology has also been utilized to investigate mucosal microvascular blood supply associated with colonic neoplasia [79]. A schematic diagram for a typical 4D-ELF system is shown in Fig. 2.

D. Angle-Resolved Low-Coherence Interferometry

In addition to providing scattering information, spectral detection of light may be used in an interferometry scheme to provide coherence-gated localization of scatterer depth in tissue. Angle-resolved low-coherence interferometry (a/LCI) is a technique that implements angle-resolved backscattering detection via Fourier-domain spatial detection of angular scattering with depth resolution utilizing low-coherence interferometry. Early a/LCI studies used the coherence-gated scattering distribution to determine the fractal organization of a cell monolayer [80]. More commonly, the angular scattering profile from a/LCI can be compared with lookup tables of angular scattering profiles derived from Mie theory to quantify the nuclear morphology from the basal layer of the epithelium during neoplastic transformation [81,82].

a/LCI has enjoyed a wealth of success in diagnosing dysplasia in the clinic, with standalone systems developed for detecting esophageal [83,84], intestinal [85], and cervical dysplasia [66,86]. In the clinical studies, repeated optical biopsies were taken with the a/LCI instrument and compared to histopathological analysis of co-registered tissue biopsies. Here, a/LCI demonstrated high sensitivity, specificity, and negative predictive value (NPV) in detecting dysplasia (92.9% sensitivity, 83.6% specificity, 98.2% NPV in the esophagus; 100% sensitivity, 97% specificity, and 100% NPV in the cervix). In addition, recent developments have incorporated scanning capability [87] and co-registered OCT imaging [88] to improve the clinical application of a/LCI. a/LCI was further developed to detect angular scattering across a

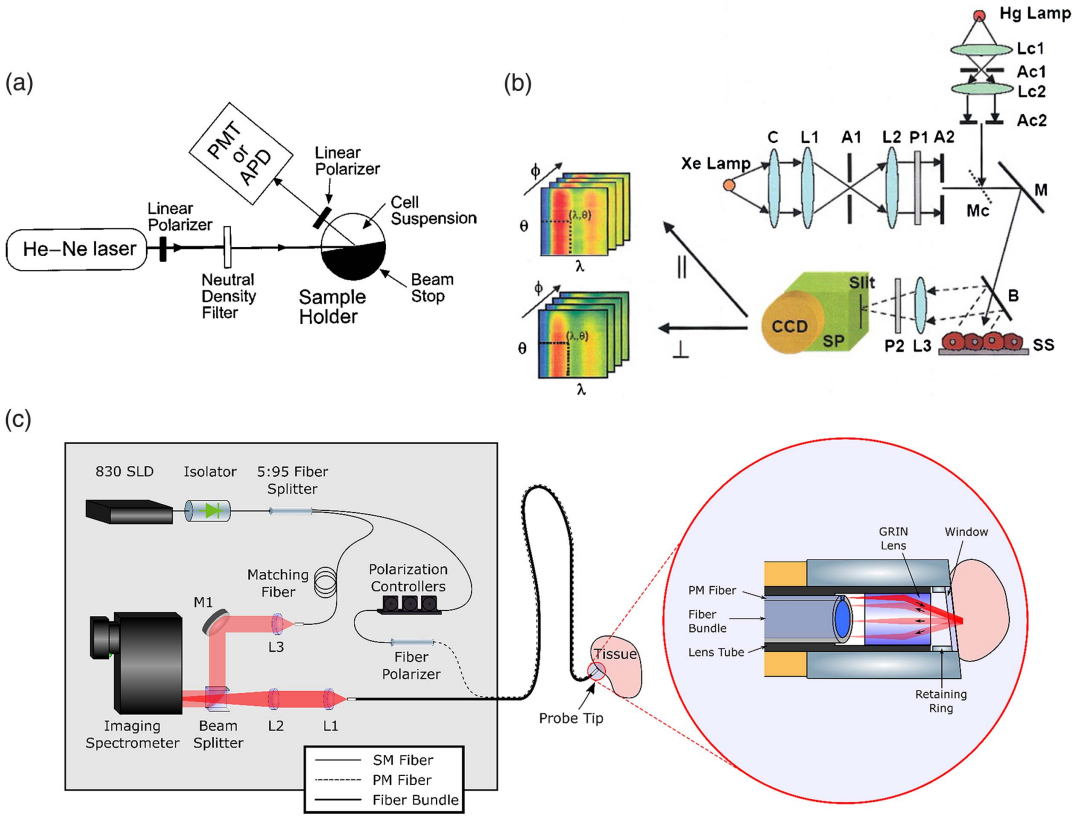

Fig. 2. Instruments for studying angular scattering from cellular and tissue samples: (A) goniometric system, (B) four-dimensional elastic light-scattering fingerprints, and (C) angle-resolved low-coherence interferometry. Reproduced with permission from Refs. [61,65,66] 2002, 2011 SPIE and 2004, Elsevier.

two-dimensional solid angle for determining the aspect ratio and orientation of spheroidal scatterers and for measuring spatial correlation distances of scatterers within tissue [88–90]. A schematic diagram of a typical a/LCI instrument is shown in Fig. 2(c).

4. FOURIER-DOMAIN METHODS

Fourier-domain techniques present an alternative to the direct measurement of scattering angles. As a general rule, the angle and position of a collection of scatterers in a sample plane are fully characterized by a transfer function. Interrogating the spatial frequency response of a sample is therefore equivalent to measuring its angular profile under certain assumptions and conditions. Several such techniques have been utilized to perform scattering measurements in cells and tissue.

A. Fourier Transform Light Scattering

Fourier transform light scattering (FTLS) was first reported by Ding *et al.* in 2008 [8]. FTLS uses diffraction phase microscopy (DPM) [93] to acquire a wavefront image near the image plane of the microscope. The acquired wavefront image is complex, including both phase and amplitude information from the sample. The scatterers in the sample plane impart a perturbation to the wavefront. A simple Fourier transform of this field is equivalent to optically propagating the scattered light and analyzing the scattered field as a function of angle.

The main advantages of FTLS are the ability to obtain scattering information from a small number of cells and, relatedly, the ability to produce scattering maps with high spatial resolution. These features allow FTLS to be used with sparse cells such as red blood cells [8]. Further, the imaging-based approach of FTLS allows the scattering signal from non-isotropic cells to be individually rotated into alignment and summed, which would not be possible with bulk scattering measurements.

Jo *et al.* used FTLS to characterize the scattering of rod-shaped bacteria, finding significant differences between the 2D scattering profiles of four superficially similar bacterial species [94]. These studies were expanded to identify unknown bacteria by feeding their FTLS-derived scattering profiles into a principal component analysis classifier, obtaining an overall classification accuracy of over 94% [95]. This FTLS-based bacterial assay could potentially be used to rapidly identify bacteria without the need for stains or labels.

Other *in vitro* models have benefited from the high-resolution dynamic scattering analysis provided by FTLS. The transport dynamics of an *in vitro* neural cell culture were characterized by Mir *et al.* [96]. In this work, the spatial correlation of subcellular structures was measured by obtaining the power spectrum of the Fourier-domain image, which is related to the autocorrelation of the complex field by the Wiener–Khinchin theorem. Mir *et al.* utilized these techniques to measure neurons during growth, finding that distinct periods of growth exist with quantitative differences in behavior [96]. The idea of examining properties of the Fourier-domain image is similar to optical scatter imaging (OSI), in which a digital micromirror device in the Fourier place enables characterization of particle shape, orientation, and aspect

ratio [97]. OSI has also been applied to study the fragmentation of mitochondria during apoptosis [98].

FTLS has also been demonstrated in tissue samples. Shortly after introducing the FTLS method, Ding *et al.* explored the scattering profiles of 5 μm thick slices of rat kidney, liver, and brain tissue and found significant differences in scattering and transport mean-free paths derived from the cross sections measured by FTLS [99]. More recently, Lee *et al.* used FTLS to map the scattering coefficient and anisotropy in the grey and white matter of both healthy and Alzheimer's diseased mouse brains [100]. FTLS in tissue is generally limited, however, to analysis of thin slices. Without being able to scan living tissue, the high temporal resolution of FTLS is not fully utilized.

B. Spatial Frequency-Domain Imaging

Another light-scattering method takes a somewhat reversed approach to FTLS. Spatial frequency-domain imaging (SFDI), first introduced by Cuccia *et al.* in 2005 [101], encodes frequency-domain interrogation into the illumination. A series of sinusoidal stripes of varying frequency are projected onto a sample using a spatial light modulator (SLM) or digital micromirror device (DMD). The light scattered within and reflected from the sample is imaged to a camera. However, each frequency of illumination does not penetrate equally into the sample. Higher frequencies are attenuated more readily due to scattering, while lower frequencies achieve greater penetration. Analyzing the input frequency response therefore reveals scattering properties as a function of depth, allowing SFDI to yield tomographic volumes of scattering data [101]. SFDI can also be performed with multiple wavelengths of light to capture color-dependent scattering and absorption properties, enabling measurement of spectrally evident properties, such as blood oxygenation [102].

Compared to many other techniques for assessing light scattering, SFDI is more amenable towards implementation in clinical settings. By performing imaging in the reflective direction and requiring only basic structural modulations of the illumination, a SFDI system can acquire its data as an external device pointed towards the sample tissue, lending itself readily to clinical translation. The authors of the original SFDI manuscript extended their original phantom study towards *in vivo* imaging of human skin and subcutaneous tissue in 2009 [92].

Unsurprisingly, SFDI finds many applications in dermatology, as many skin disorders benefit from a quantitative picture of subcutaneous tissue. SFDI has been used to evaluate burn severity [103], to identify patients at risk of developing pressure ulcers [104], and to characterize the cancer risk of actinic skin lesions [105].

SFDI is also being used to discriminate tumors and tumor margins based on the distinct scattering properties of cancerous tissue. Rohrbach *et al.* used SFDI to map skin cancer tumors by absorption, scattering, blood oxygen saturation, and hemoglobin [106]. McClatchy *et al.* found that SFDI could classify stroma, epithelium, and adipose tissue in *ex vivo* human breast tissue that were well validated against histology [107].

The brain presents an even greater challenge for subsurface imaging, though various groups have explored using SFDI for neurobiology. An SFDI study of a mouse model of Alzheimer's was able to detect significant differences in the wavelength-dependent scattering and absorption of the brain between control and disease states, even when imaging *in vivo* through the intact skull [108]. By extracting absorption cross sections, SFDI has also been used to image drug delivery in rat brains [109]. Changes in tissue absorption and scattering due to hypoxic injury have also enabled SFDI study of the damage to rat brains resulting from cardiac arrest [110]. A block diagram showing SFDI instrumentation is shown in Fig. 3.

It should be noted that many implementations of SFDI rely on adaptations of the diffusion theory of photon propagation, in contrast to many of the techniques discussed in this review, which operate using primarily single-scattered photons. Bridging this gap, Kanick *et al.* have used high-spatial-frequency illumination to isolate light in the sub-diffuse transport regime [111] with observed differences between normal and scar tissue in a healthy volunteer. Further examination of the assumptions inherent to photon propagation models in SFDI would be of great interest to the broader optics community.

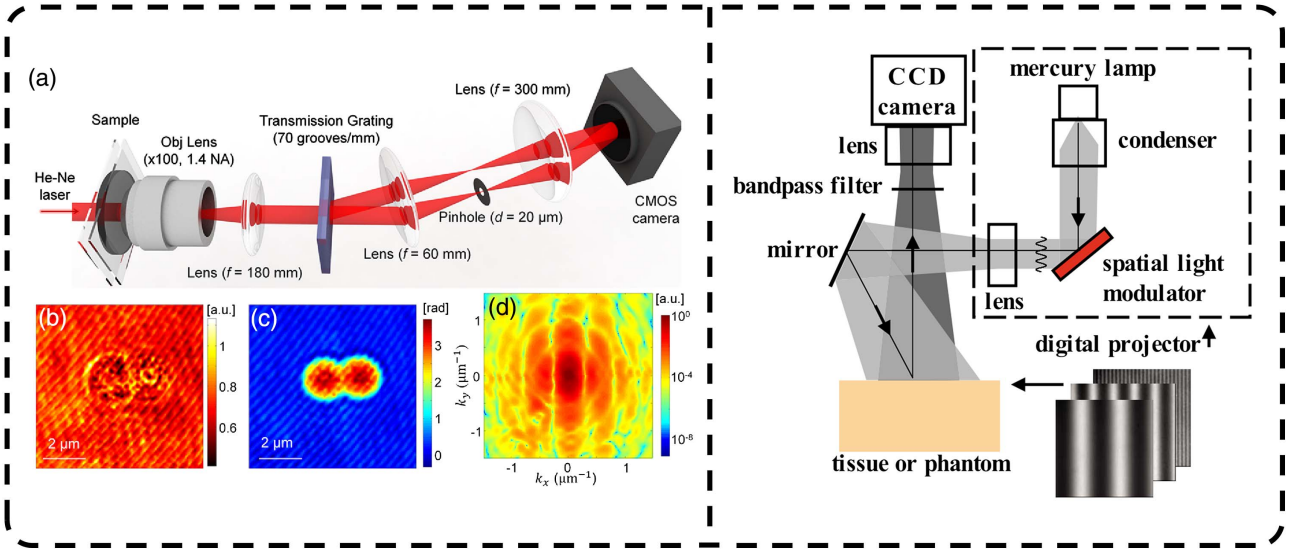

Fig. 3. (Left) (a) Setup for diffraction phase microscopy, which enables Fourier-transform light scattering, (b) amplitude image, and (c) phase maps of polymethyl methacrylate spheres, with (d) the associated light-scattering pattern computed from the phase image. (Right) Instrumentation schematic for spatial frequency-domain imaging. Reproduced with permission from Refs. [91,92] 2012, The Optical Society and 2009, SPIE.

5. DISCUSSION

A comprehensive index of the techniques discussed in this review is shown in Table 1. For a substantial portion of these techniques, a familiar pattern emerges. First, a mathematical model of varying complexity is developed to model tissue scattering. Next, a physical property associated with a variable in the model is measured, and the data are fitted to a library of model variations until a best fit is found. This general framework is present in some form in ESS, LSS, diffuse reflectance modeling, ISOCT, and a/LCI, among others, and allows for measurement of quantities that are difficult to access, as when partial-wave spectroscopy demonstrates sensitivity to correlations at the nanoscale [112] despite these features existing an order of magnitude or more below the diffraction limit. As always, limitations should be acknowledged. In particular, this procedure constrains the range and resolution of possible measurements to a pre-computed class of model outcomes defined by an array of input variables. These models make assumptions regarding tissue morphology, composition, scatterer size and shape, and optical properties that are generally accurate but may not countenance statistical variations in patients or tissues. In some cases, these assumptions may be simply incorrect, as assumptions of the nuclear refractive index increasingly appear to have been [67,68,113]. Deviations from the assumed simplicity of analytic models may produce errors in analysis and ultimately limit device performance over large populations. Such limitations are not often identified in preliminary studies, but in truth may contribute heavily to the ultimate clinical effectiveness of these techniques.

One potential solution to the issues inherent in model fitting is machine learning. Analytic models may be insufficiently complex (or overly complex), imbalanced in certain variables, or improperly characterize the real-world range of parameters. Instead, any series of measurements can simply be entered into a machine learning algorithm, which will find the optimum discriminatory variables in high-dimensional space. While obviously an effective strategy, machine learning approaches should take care that they are not overfitting to a particular dataset at the expense of a more generalizable diagnostic. Prospective validation studies (in which classifications are based on parameter cutoffs from previous studies) are underrepresented in the literature, and execution of such studies should help prevent machine learning classifiers that are accurate for the case of a small feasibility study but not valid for larger populations.

Many analytic models of light scattering take extreme caution in developing complex theory to explain the scattering process. Less care is generally taken when assuming physical constants,

Table 1. Summary of Biomedical Light Scattering Techniques

Technique	Contrast Mechanism	Representative Applications in Tissue
Elastic-scattering spectroscopy (ESS)	Spectral	Bladder Cancer [11]; Breast cancer [12]; Colonic lesions [13]; Dysplastic Barrett's esophagus [14]; Malignancy in *ex vivo* thyroid [17]; Colonic polyps [18]; Skin lesions [19]; Dysplastic and inflammatory prostate *ex vivo* [11,15].
Diffuse reflectance spectroscopy	Spectral	Skin cancer [21]; Breast surgical margin analysis [22]; Peripheral lung tumors [23].
Light-scattering spectroscopy (LSS)	Spectral, Polarization	Dysplastic Barrett's esophagus [5,28–30]; Field carcinogenesis (rat model) [24]; Colonic adenoma [25]; EIBS during colon carcinogenesis [26]; EIBS associated with neoplastic pancreatic lesions [31]; Malignant potential of pancreatic cystic lesions [32].
Diffuse reflectance modeling	Spectral	Normal and adenomatous colon *in vivo* [34]
Spectroscopic OCT (SOCT)	Spectral, Depth-resolved (Interferometric)	Carcinogenesis in the pancreas and colon [42]; Burn severity [43]; Retinal oximetry [44]; Microvascular hemoglobin mapping [45]; Amyloid beta plaques in the human and mouse brain [46]; Bilirubin quantification [47]; Light scattering spectroscopy of the retina [48]; Colon cancer *ex vivo* [49].
Dark-field spectral scatter imaging	Spectral	Breast surgical margins [51]; Various breast pathologies [52].
Partial wave spectroscopy (PWS)	Spectral	Field carcinogenesis in the colon, pancreas, and lung [55]; Cytological brushings of the rectal mucosa [56];
Goniometric measurements	Angle-resolved	Morphological structure of organelles [59–61]; Multicellular spheroids [62,63]; DNA content [64].
Finite-difference time-domain (FDTD) methods	Angle-resolved	Nuclear size and refractive index [74,75]; Collagen fiber networks [76]; Epithelial depth [77];
Four-dimensional elastic light-scattering fingerprinting (4D-ELF)	Spectral, Angle-resolved, Azimuthal, Polarization	Colon carcinogenesis (rat model) [65,78]; Early carcinogenesis of the rectal mucosa [79].
Angle-resolved low-coherence interferometry (a/LCI)	Angle-resolved, Depth-resolved (Interferometric)	Esophageal dysplasia [83,84]; Intestinal dysplasia [85]; Cervical dysplasia [66,86]; Grading of esophageal neoplasia (rat model) [82]; Esophageal adenocarcinoma (rat model) and retinal degradation (mouse model) [88];
Fourier transform light scattering (FTLS)	Fourier-domain, Angle-resolved	Identification of bacterial species [94,95]; Neural transport and growth dynamics [96]; Alzheimer's disease (mouse model) [100].
Spatial frequency-domain imaging (SFDI)	Fourier-domain, Spectral	Blood oxygenation [102]; Burn severity [103]; Pressure ulcer risk assessment [104]; Cancer risk of actinic skin lesions [105]; Skin cancer [106]; Breast tissue classification [107]; Alzheimer's disease (mouse model) [108]; Brain damage from cardiac arrest (mouse model) [110].

with many works content to pull parameters related to refractive index, size distribution, and nucleus-to-cytoplasm ratio from decades-old studies [114,115]. There is a general dearth of basic research related to the statistical presentation of scattering properties, including variation on the temporal and spatial scales and across cell lines and types. Emerging technologies like refractive-index tomography [116,117] as well as more established techniques like digital holographic microscopy [118,119] are well suited to this type of characterization. This type of work is labor intensive and often underappreciated, but an improved body of knowledge regarding the optical properties of biological specimens would provide a more solid foundation for models of tissue scattering.

Computational resources have improved markedly in recent years; however, it is not obvious that an accompanying renaissance in numerical light-scattering studies, such as FDTD modeling, has occurred. This is particularly interesting given the additional advances in parallel computing and GPU-based processing in this time period. While the exact reason is unclear, we can speculate that further simulations of light scattering from homogenous tissue models may be uninteresting and also have been shown to exhibit results heavily dependent on initial assumptions of the phase function and other parameters [37]. A potential avenue of new research exists in creating more realistic models of cells and tissues using quantitative measurements. Comparisons of light scattering between realistic models of cellular architecture and simplified models would provide a stronger empirical backing for the use of simplified models and further legitimize diagnostic modalities that rely on light scattering.

Substantial innovation in the field of scattering-based optical diagnostics continues to occur at the level of basic research, and considerable support for established technologies like OCT is available within commercialized entities. However, there is a dearth of movement between the two spaces, with a number of optical technologies unable to realize commercial success despite substantial success in clinical studies. A portion of this stasis is likely related to mandatory regulatory pathways defined by the U.S. Food and Drug Administration (FDA), in which devices lacking a cleared predicate are required to undergo Premarket Approval (PMA). The PMA process can require a substantial investment, with years of time and significant expenditure before completion. Recent adoption of the *de novo* process by the FDA promises to enable a more accessible pathway for Class I devices, similar to the less burdensome 510(k) process. Further innovations in regulatory pathways, such as specialized pathways for low-risk photonic diagnostics, may incentivize the formation of new companies and ventures around these techniques.

A common theme in many of the studies discussed in this review is the comparison of a specific measurement technique with the "gold standard" of histopathology, the premise being that scattering-based diagnostics should match the classification of a representative biopsy examined by an expert pathologist. Histopathology is a tried and true method, and it has remained the standard of care in essentially all branches of medicine for over a century. However, it is also not without limitations, with issues including sampling error and relatively high inter-observer variability (<50% agreement) for some conditions like esophageal dysplasia [120]. On the occasion when an optical technique is sensitive to pathology that is not discovered by a biopsy, a comparative study would classify this as a failure of the optical technology rather than a failure of the pathologist. Extending such validation studies to include supplemental techniques such as immunohistochemistry [121] and genomic screening will help improve validation of new photonic diagnostic devices.

This review has focused primarily on elastic scattering; however, a significant literature on inelastic scattering exists as well. Diagnostic modalities based on Raman scattering have been quite popular over the years [122–124], and Brillouin spectroscopy has seen a recent increase in interest driven primarily by improved spectrometer technology [125–127]. Regulatory pathway reform may help to incentivize commercialization of these technologies as well.

6. CONCLUSION

In this review, we have given an examination of the current state of photonic technologies that utilize light scattering for disease detection. Techniques that measure spectral, angular, and phase properties of the scattered field have been presented, along with examinations of the associated instrumentation and data processing schemes. A discussion of the state of the field was presented. Rich innovation on the level of basic research, combined with prudent regulatory reform and continued investment in translational studies, will allow for continued success in the years to come.

Funding. National Institutes of Health (NIH) (R01 CA167421, R01 CA210544); National Science Foundation (NSF).

Acknowledgment. Z. S. gratefully acknowledges support from the NSF-GRFP program.

DISCLOSURES

A. W.: Lumedica, Inc. (I,P).

REFERENCES

1. A. Wax and V. Backman, *Biomedical Applications of Light Scattering* (McGraw Hill Professional, 2009).
2. H. C. van de Hulst, *Light Scattering by Small Particles* (Courier Corporation, 1957).
3. A. Ishimaru, *Wave Propagation and Scattering in Random Media* (Wiley, 1999).
4. G. Mie, "Beiträge zur optik trüber medien, speziell kolloidaler metallösungen," Ann. Phys. **330**, 377–445 (1908).
5. L. Perelman, V. Backman, M. Wallace, G. Zonios, R. Manoharan, A. Nusrat, S. Shields, M. Seiler, C. Lima, T. Hamano, I. Itzkan, J. Van Dam, J. M. Crawford, and M. S. Feld, "Observation of periodic fine structure in reflectance from biological tissue: a new technique for measuring nuclear size distribution," Phys. Rev. Lett. **80**, 627–630 (1998).
6. A. Wax, C. Yang, M. G. Müller, R. Nines, C. W. Boone, V. E. Steele, G. D. Stoner, R. R. Dasari, and M. S. Feld, "In situ detection of neoplastic transformation and chemopreventive effects in rat esophagus epithelium using angle-resolved low-coherence interferometry," Cancer Res. **63**, 3556–3559 (2003).
7. J. F. De Boer, T. E. Milner, M. J. van Gemert, and J. S. Nelson, "Two-dimensional birefringence imaging in biological tissue by polarization-sensitive optical coherence tomography," Opt. Lett. **22**, 934–936 (1997).
8. H. Ding, Z. Wang, F. Nguyen, S. A. Boppart, and G. Popescu, "Fourier transform light scattering of inhomogeneous and dynamic structures," Phys. Rev. Lett. **101**, 238102 (2008).
9. D. Huang, E. A. Swanson, C. P. Lin, J. S. Schuman, W. G. Stinson, W. Chang, M. R. Hee, T. Flotte, K. Gregory, and C. A. Puliafito, "Optical coherence tomography," Science **254**, 1178–1181 (1991).
10. M. T. Rinehart, H. S. Park, and A. Wax, "Influence of defocus on quantitative analysis of microscopic objects and individual cells with digital holography," Biomed. Opt. Express **6**, 2067–2075 (2015).
11. J. R. Mourant, I. J. Bigio, J. Boyer, R. L. Conn, T. Johnson, and T. Shimada, "Spectroscopic diagnosis of bladder cancer with elastic light scattering," Lasers Surg. Med. **17**, 350–357 (1995).

12. I. J. Bigio, S. G. Bown, G. Briggs, C. Kelley, S. Lakhani, D. Pickard, P. M. Ripley, I. G. Rose, and C. Saunders, "Diagnosis of breast cancer using elastic-scattering spectroscopy: preliminary clinical results," J. Biomed. Opt. **5**, 221–229 (2000).
13. A. Dhar, K. S. Johnson, M. R. Novelli, S. G. Bown, I. J. Bigio, L. B. Lovat, and S. L. Bloom, "Elastic scattering spectroscopy for the diagnosis of colonic lesions: initial results of a novel optical biopsy technique," Gastrointestinal Endoscopy **63**, 257–261 (2006).
14. L. B. Lovat, K. Johnson, G. D. Mackenzie, B. R. Clark, M. R. Novelli, S. Davies, M. O'Donovan, C. Selvasekar, S. M. Thorpe, D. Pickard, R. Fitzgerald, T. Fearn, I. Bigio, and S. G. Bown, "Elastic scattering spectroscopy accurately detects high grade dysplasia and cancer in Barrett's oesophagus," Gut **55**, 1078–1083 (2006).
15. O. A'amar, L. Liou, E. Rodriguez-Diaz, A. De las Morenas, and I. Bigio, "Comparison of elastic scattering spectroscopy with histology in ex vivo prostate glands: potential application for optically guided biopsy and directed treatment," Laser Med. Sci. **28**, 1323–1329 (2013).
16. R. Reif, M. S. Amorosino, K. W. Calabro, O. M. Aamar, S. K. Singh, and I. J. Bigio, "Analysis of changes in reflectance measurements on biological tissues subjected to different probe pressures," Proc. SPIE **13**, 3 (2008).
17. H. Suh, O. A'amar, E. Rodriguez-Diaz, S. Lee, I. Bigio, and J. E. Rosen, "Elastic light-scattering spectroscopy for discrimination of benign from malignant disease in thyroid nodules," Ann. Surg. Oncol. **18**, 1300–1305 (2011).
18. E. Rodriguez-Diaz, Q. Huang, S. R. Cerda, M. J. O'Brien, I. J. Bigio, and S. K. Singh, "Endoscopic histological assessment of colonic polyps by using elastic scattering spectroscopy," Gastrointestinal Endoscopy **81**, 539–547 (2015).
19. T. Upile, W. Jerjes, H. Radhi, J. Mahil, A. Rao, and C. Hopper, "Elastic scattering spectroscopy in assessing skin lesions: an 'in vivo' study," Photodiagn. Photodyn. Ther. **9**, 132–141 (2012).
20. I. J. Bigio and J. R. Mourant, "Ultraviolet and visible spectroscopies for tissue diagnostics: fluorescence spectroscopy and elastic-scattering spectroscopy," Phys. Med. Biol. **42**, 803–814 (1997).
21. A. Garcia-Uribe, J. Zou, M. Duvic, J. H. Cho-Vega, V. G. Prieto, and L. V. Wang, "In vivo diagnosis of melanoma and nonmelanoma skin cancer using oblique incidence diffuse reflectance spectrometry," Cancer Res. **72**, 2738–2745 (2012).
22. M. D. Keller, S. K. Majumder, M. C. Kelley, I. M. Meszoely, F. I. Boulos, G. M. Olivares, and A. Mahadevan-Jansen, "Autofluorescence and diffuse reflectance spectroscopy and spectral imaging for breast surgical margin analysis," Lasers Surg. Med. **42**, 15–23 (2010).
23. J. W. Spliethoff, D. J. Evers, H. M. Klomp, J. W. van Sandick, M. W. Wouters, R. Nachabe, G. W. Lucassen, B. H. Hendriks, J. Wesseling, and T. J. Ruers, "Improved identification of peripheral lung tumors by using diffuse reflectance and fluorescence spectroscopy," Lung Cancer **80**, 165–171 (2013).
24. A. J. Gomes, S. K. Ruderman, V. Backman, M. D. Cruz, R. K. Wali, and H. K. Roy, "In vivo measurement of the shape of the tissue-refractive-index correlation function and its application to detection of colorectal field carcinogenesis," J. Biomed. Opt. **17**, 047005 (2012).
25. R. S. Gurjar, V. Backman, L. T. Perelman, I. Georgakoudi, K. Badizadegan, I. Itzkan, R. R. Dasari, and M. S. Feld, "Imaging human epithelial properties with polarized light-scattering spectroscopy," Nat. Med. **7**, 1245–1248 (2001).
26. M. P. Siegel, Y. L. Kim, H. K. Roy, R. K. Wali, and V. Backman, "Assessment of blood supply in superficial tissue by polarization-gated elastic light-scattering spectroscopy," Appl. Opt. **45**, 335–342 (2006).
27. V. Backman, V. Gopal, M. Kalashnikov, K. Badizadegan, R. Gurjar, A. Wax, I. Georgakoudi, M. Mueller, C. W. Boone, R. R. Dasari, and M. S. Feld, "Measuring cellular structure at submicrometer scale with light scattering spectroscopy," IEEE J. Sel. Top. Quantum Electron. **7**, 887–893 (2001).
28. I. Georgakoudi, B. C. Jacobson, J. Van Dam, V. Backman, M. B. Wallace, M. G. Müller, Q. Zhang, K. Badizadegan, D. Sun, G. A. Thomas, L. T. Perelman, and M. S. Feld, "Fluorescence, reflectance, and light-scattering spectroscopy for evaluating dysplasia in patients with Barrett's esophagus," Gastroenterology **120**, 1620–1629 (2001).
29. L. Qiu, D. K. Pleskow, R. Chuttani, E. Vitkin, J. Leyden, N. Ozden, S. Itani, L. Guo, A. Sacks, J. D. Goldsmith, M. D. Modell, E. B. Hanlon, I. Itzkan, and L. T. Perelman, "Multispectral scanning during endoscopy guides biopsy of dysplasia in Barrett's esophagus," Nat. Med. **16**, 603–606 (2010).
30. L. Qiu, R. Chuttani, D. K. Pleskow, V. Turzhitsky, U. Khan, Y. N. Zakharov, L. Zhang, T. M. Berzin, E. U. Yee, M. S. Sawhney, Y. Li, E. Vitkin, J. D. Goldsmith, I. Itzkan, and L. T. Perelman, "Multispectral light scattering endoscopic imaging of esophageal precancer," Light: Sci. Appl. **7**, 17174 (2018).
31. M. Patel, A. Gomes, S. Ruderman, D. Hardee, S. Crespo, M. Raimondo, T. Woodward, V. Backman, H. Roy, and M. Wallace, "Polarization gating spectroscopy of normal-appearing duodenal mucosa to detect pancreatic cancer," Gastrointestinal Endoscopy **80**, 786–793.e2 (2014).
32. L. Zhang, D. K. Pleskow, V. Turzhitsky, E. U. Yee, T. M. Berzin, M. Sawhney, S. Shinagare, E. Vitkin, Y. Zakharov, U. Khan, F. Wang, J. D. Goldsmith, S. Goldberg, R. Chuttani, I. Itzkan, L. Qiu, and L. T. Perelman, "Light scattering spectroscopy identifies the malignant potential of pancreatic cysts during endoscopy," Nat. Biomed. Eng. **1**, 0040 (2017).
33. T. J. Farrell, M. S. Patterson, and B. Wilson, "A diffusion theory model of spatially resolved, steady-state diffuse reflectance for the noninvasive determination of tissue optical properties in vivo," Med. Phys. **19**, 879–888 (1992).
34. G. Zonios, L. T. Perelman, V. Backman, R. Manoharan, M. Fitzmaurice, J. Van Dam, and M. S. Feld, "Diffuse reflectance spectroscopy of human adenomatous colon polyps in vivo," Appl. Opt. **38**, 6628–6637 (1999).
35. G. Zonios and A. Dimou, "Modeling diffuse reflectance from homogeneous semi-infinite turbid media for biological tissue applications: a Monte Carlo study," Biomed. Opt. Express **2**, 3284–3294 (2011).
36. G. Mantis and G. Zonios, "Simple two-layer reflectance model for biological tissue applications," Appl. Opt. **48**, 3490–3496 (2009).
37. K. W. Calabro and I. J. Bigio, "Influence of the phase function in generalized diffuse reflectance models: review of current formalisms and novel observations," J. Biomed. Opt. **19**, 075005 (2014).
38. U. Morgner, C. Xu, and S. A. Boppart, "Spectroscopic optical coherence tomography," Opt. Lett. **25**, 111–113 (2000).
39. F. Robles, R. N. Graf, and A. Wax, "Dual window method for processing spectroscopic optical coherence tomography signals with simultaneously high spectral and temporal resolution," Opt. Express **17**, 6799–6812 (2009).
40. F. E. Robles, C. Wilson, G. Grant, and A. Wax, "Molecular imaging true-colour spectroscopic optical coherence tomography," Nat. Photonics **5**, 744–747 (2011).
41. J. Yi and V. Backman, "Imaging a full set of optical scattering properties of biological tissue by inverse spectroscopic optical coherence tomography," Opt. Lett. **37**, 4443–4445 (2012).
42. J. Yi, A. J. Radosevich, Y. Stypula-Cyrus, N. N. Mutyal, S. M. Azarin, E. Horcher, M. J. Goldberg, L. Bianchi, S. Bajaj, H. K. Roy, and V. Backman, "Spatially resolved optical and ultrastructural properties of colorectal and pancreatic field carcinogenesis observed by inverse spectroscopic optical coherence tomography," J. Biomed. Opt. **19**, 036013 (2014).
43. Y. Zhao, J. R. Maher, J. Kim, M. A. Selim, H. Levinson, and A. Wax, "Evaluation of burn severity in vivo in a mouse model using spectroscopic optical coherence tomography," Biomed. Opt. Express **6**, 3339–3345 (2015).
44. J. Yi, Q. Wei, W. Liu, V. Backman, and H. F. Zhang, "Visible-light optical coherence tomography for retinal oximetry," Opt. Lett. **38**, 1796–1798 (2013).
45. S. P. Chong, C. W. Merkle, C. Leahy, H. Radhakrishnan, and V. J. Srinivasan, "Quantitative microvascular hemoglobin mapping using visible light spectroscopic optical coherence tomography," Biomed. Opt. Express **6**, 1429–1450 (2015).
46. A. Lichtenegger, D. J. Harper, M. Augustin, P. Eugui, M. Muck, J. Gesperger, C. K. Hitzenberger, A. Woehrer, and B. Baumann, "Spectroscopic imaging with spectral domain visible light optical coherence microscopy in Alzheimer's disease brain samples," Biomed. Opt. Express **8**, 4007–4025 (2017).
47. C. Veenstra, W. Petersen, I. M. Vellekoop, W. Steenbergen, and N. Bosschaart, "Spatially confined quantification of bilirubin concentrations by spectroscopic visible-light optical coherence tomography," Biomed. Opt. Express **9**, 3581–3589 (2018).
48. W. Song, L. Zhou, S. Zhang, S. Ness, M. Desai, and J. Yi, "Fiber-based visible and near infrared optical coherence tomography (vnOCT) enables quantitative elastic light scattering spectroscopy in human retina," Biomed. Opt. Express **9**, 3464–3480 (2018).

49. M. Kassinopoulos, E. Bousi, I. Zouvani, and C. Pitris, "Correlation of the derivative as a robust estimator of scatterer size in optical coherence tomography (OCT)," Biomed. Opt. Express **8**, 1598–1606 (2017).
50. V. Krishnaswamy, A. M. Laughney, K. D. Paulsen, and B. W. Pogue, "Dark-field scanning in situ spectroscopy platform for broadband imaging of resected tissue," Opt. Lett. **36**, 1911–1913 (2011).
51. A. M. Laughney, V. Krishnaswamy, E. J. Rizzo, M. C. Schwab, R. J. Barth, B. W. Pogue, K. D. Paulsen, and W. A. Wells, "Scatter spectroscopic imaging distinguishes between breast pathologies in tissues relevant to surgical margin assessment," Clin. Cancer Res. **18**, 6315–6325 (2012).
52. V. Krishnaswamy, A. M. Laughney, W. A. Wells, K. D. Paulsen, and B. W. Pogue, "Scanning in situ spectroscopy platform for imaging surgical breast tissue specimens," Opt. Express **21**, 2185–2194 (2013).
53. H. Subramanian, P. Pradhan, Y. Liu, I. R. Capoglu, J. D. Rogers, H. K. Roy, R. E. Brand, and V. Backman, "Partial-wave microscopic spectroscopy detects subwavelength refractive index fluctuations: an application to cancer diagnosis," Opt. Lett. **34**, 518–520 (2009).
54. H. Subramanian, P. Pradhan, Y. Liu, I. R. Capoglu, X. Li, J. D. Rogers, A. Heifetz, D. Kunte, H. K. Roy, A. Taflove, and V. Backman, "Optical methodology for detecting histologically unapparent nanoscale consequences of genetic alterations in biological cells," Proc. Natl. Acad. Sci. USA **105**, 20118–20123 (2008).
55. H. Subramanian, P. Pradhan, Y. Liu, I. R. Capoglu, X. Li, J. D. Rogers, A. Heifetz, D. Kunte, H. K. Roy, A. Taflove, and V. Backman, "Nanoscale cellular changes in field carcinogenesis detected by partial wave spectroscopy," Cancer Res. **69**, 5357–5363 (2009).
56. V. Backman and H. K. Roy, "Light-scattering technologies for field carcinogenesis detection: a modality for endoscopic prescreening," Gastroenterology **140**, 35–41.e5 (2011).
57. J. S. Kim, P. Pradhan, V. Backman, and I. Szleifer, "The influence of chromosome density variations on the increase in nuclear disorder strength in carcinogenesis," Phys. Biol. **8**, 015004 (2011).
58. D. Damania, H. Subramanian, A. K. Tiwari, Y. Stypula, D. Kunte, P. Pradhan, H. K. Roy, and V. Backman, "Role of cytoskeleton in controlling the disorder strength of cellular nanoscale architecture," Biophys. J. **99**, 989–996 (2010).
59. J. R. Mourant, J. P. Freyer, A. H. Hielscher, A. A. Eick, D. Shen, and T. M. Johnson, "Mechanisms of light scattering from biological cells relevant to noninvasive optical-tissue diagnostics," Appl. Opt. **37**, 3586–3593 (1998).
60. R. Drezek, A. Dunn, and R. Richards-Kortum, "Light scattering from cells: finite-difference time-domain simulations and goniometric measurements," Appl. Opt. **38**, 3651–3661 (1999).
61. J. R. Mourant, T. M. Johnson, S. Carpenter, A. Guerra, T. Aida, and J. P. Freyer, "Polarized angular dependent spectroscopy of epithelial cells and epithelial cell nuclei to determine the size scale of scattering structures," J. Biomed. Opt. **7**, 378–387 (2002).
62. J. R. Mourant, T. M. Johnson, V. Doddi, and J. P. Freyer, "Angular dependent light scattering from multicellular spheroids," J. Biomed. Opt. **7**, 93–99 (2002).
63. R. Ceolato, N. Riviere, R. Jorand, B. Ducommun, and C. Lorenzo, "Light-scattering by aggregates of tumor cells: spectral, polarimetric, and angular measurements," J. Quant. Spectrosc. Radiat. Transfer **146**, 207–213 (2014).
64. X. Lin, N. Wan, L. Weng, and Y. Zhou, "Angular-dependent light scattering from cancer cells in different phases of the cell cycle," Appl. Opt. **56**, 8154–8158 (2017).
65. H. K. Roy, Y. Liu, R. K. Wali, Y. L. Kim, A. K. Kromine, M. J. Goldberg, and V. Backman, "Four-dimensional elastic light-scattering fingerprints as preneoplastic markers in the rat model of colon carcinogenesis," Gastroenterology **126**, 1071–1081 (2004).
66. D. Ho, T. K. Drake, R. C. Bentley, F. A. Valea, and A. Wax, "Evaluation of hybrid algorithm for analysis of scattered light using ex vivo nuclear morphology measurements of cervical epithelium," Biomed. Opt. Express **6**, 2755–2765 (2015).
67. Z. A. Steelman, W. J. Eldridge, and A. Wax, "Response to Comment on 'Is the nuclear refractive index lower than cytoplasm? Validation of phase measurements and implications for light scattering technologies'," J. Biophoton. **11**, e201800091 (2018).
68. Z. A. Steelman, W. J. Eldridge, J. B. Weintraub, and A. Wax, "Is the nuclear refractive index lower than cytoplasm? Validation of phase measurements and implications for light scattering technologies," J. Biophoton. **10**, 1714–1722 (2017).
69. R. Drezek, M. Guillaud, T. Collier, I. Boiko, A. Malpica, C. Macaulay, M. Follen, and R. Richards-Kortum, "Light scattering from cervical cells throughout neoplastic progression: influence of nuclear morphology, DNA content, and chromatin texture," J. Biomed. Opt. **8**, 7–16 (2003).
70. D. Arifler, M. Guillaud, A. Carraro, A. Malpica, M. Follen, and R. Richards-Kortum, "Light scattering from normal and dysplastic cervical cells at different epithelial depths: finite-difference time-domain modeling with a perfectly matched layer boundary condition," J. Biomed. Opt. **8**, 484–494 (2003).
71. S. E. Krakiwsky, L. E. Turner, and M. M. Okoniewski, "Graphics processor unit (GPU) acceleration of finite-difference time-domain (FDTD) algorithm," Proc. IEEE **5**, 265–268 (2004).
72. T. Nagaoka and S. Watanabe, "A GPU-based calculation using the three-dimensional FDTD method for electromagnetic field analysis," in *Annual International Conference of the IEEE Engineering in Medicine and Biology Society (EMBC)* (2010), pp. 327–330.
73. T. Nagaoka and S. Watanabe, "Accelerating three-dimensional FDTD calculations on GPU clusters for electromagnetic field simulation," in *Annual International Conference of the IEEE Engineering in Medicine and Biology Society (EMBC)* (2012), pp. 5691–5694.
74. X. Lin, N. Wan, L. Weng, and Y. Zhou, "Light scattering from normal and cervical cancer cells," Appl. Opt. **56**, 3608–3614 (2017).
75. W. C. Hsu, J. W. Su, C. C. Chang, and K. B. Sung, "Investigating the backscattering characteristics of individual normal and cancerous cells based on experimentally determined three-dimensional refractive index distributions," Proc. SPIE **8553**, 85531O (2012).
76. D. Arifler, I. Pavlova, A. Gillenwater, and R. Richards-Kortum, "Light scattering from collagen fiber networks: micro-optical properties of normal and neoplastic stroma," Biophys. J. **92**, 3260–3274 (2007).
77. D. Arifler, C. Macaulay, M. Follen, and M. Guillaud, "Numerical investigation of two-dimensional light scattering patterns of cervical cell nuclei to map dysplastic changes at different epithelial depths," Biomed. Opt. Express **5**, 485–498 (2014).
78. Y. L. Kim, Y. Liu, R. K. Wali, H. K. Roy, M. J. Goldberg, A. K. Kromin, K. Chen, and V. Backman, "Simultaneous measurement of angular and spectral properties of light scattering for characterization of tissue microarchitecture and its alteration in early precancer," IEEE J. Sel. Top. Quantum Electron. **9**, 243–256 (2003).
79. A. J. Gomes, H. K. Roy, V. Turzhitsky, Y. Kim, J. D. Rogers, S. Ruderman, V. Stoyneva, M. J. Goldberg, L. K. Bianchi, E. Yen, A. Kromine, M. Jameel, and V. Backman, "Rectal mucosal microvascular blood supply increase is associated with colonic neoplasia," Clin. Cancer Res. **15**, 3110–3117 (2009).
80. A. Wax, C. Yang, V. Backman, K. Badizadegan, C. W. Boone, R. R. Dasari, and M. S. Feld, "Cellular organization and substructure measured using angle-resolved low-coherence interferometry," Biophys. J. **82**, 2256–2264 (2002).
81. J. Pyhtila, R. Graf, and A. Wax, "Determining nuclear morphology using an improved angle-resolved low coherence interferometry system," Opt. Express **11**, 3473–3484 (2003).
82. A. Wax, J. W. Pyhtila, R. N. Graf, R. Nines, C. W. Boone, R. R. Dasari, M. S. Feld, V. E. Steele, and G. D. Stoner, "Prospective grading of neoplastic change in rat esophagus epithelium using angle-resolved low-coherence interferometry," J. Biomed. Opt. **10**, 051604 (2005).
83. N. G. Terry, N. G. Terry, Y. Zhu, S. C. Gebhart, W. J. Brown, S. D. Bright, E. E. Carretta, J. T. Woosley, and N. J. Shaheen, "Detection of dysplasia in Barrett's esophagus with angle-resolved low coherence interferometry," Gastrointestinal Endoscopy **71**, Ab121–Ab122 (2010).
84. N. G. Terry, Y. Zhu, M. T. Rinehart, W. J. Brown, S. C. Gebhart, S. Bright, E. Carretta, C. G. Ziefle, M. Panjehpour, J. Galanko, R. D. Madanick, E. S. Dellon, D. Trembath, A. Bennett, J. R. Goldblum, B. F. Overholt, J. T. Woosley, N. J. Shaheen, and A. Wax, "Detection of dysplasia in Barrett's esophagus with in vivo depth-resolved nuclear morphology measurements," Gastroenterology **140**, 42–50 (2011).
85. N. Terry, Y. Zhu, J. K. Thacker, J. Migaly, C. Guy, C. R. Mantyh, and A. Wax, "Detection of intestinal dysplasia using angle-resolved low coherence interferometry," J. Biomed. Opt. **16**, 106002 (2011).
86. D. Ho, T. K. Drake, K. K. Smith-McCune, T. M. Darragh, L. Y. Hwang, and A. Wax, "Feasibility of clinical detection of cervical dysplasia using angle-resolved low coherence interferometry measurements of depth-resolved nuclear morphology," Int. J. Cancer **140**, 1447–1456 (2017).

87. Z. A. Steelman, D. Ho, K. K. Chu, and A. Wax, "Scanning system for angle-resolved low-coherence interferometry," Opt. Lett. **42**, 4581–4584 (2017).
88. S. Kim, S. Heflin, L. A. Kresty, M. Halling, L. N. Perez, D. Ho, M. Crose, W. Brown, S. Farsiu, V. Arshavsky, and A. Wax, "Analyzing spatial correlations in tissue using angle-resolved low coherence interferometry measurements guided by co-located optical coherence tomography," Biomed. Opt. Express **7**, 1400–1414 (2016).
89. C. Amoozegar, M. G. Giacomelli, J. D. Keener, K. J. Chalut, and A. Wax, "Experimental verification of T-matrix-based inverse light scattering analysis for assessing structure of spheroids as models of cell nuclei," Appl. Opt. **48**, D20–D25 (2009).
90. M. Giacomelli, Y. Zhu, J. Lee, and A. Wax, "Size and shape determination of spheroidal scatterers using two-dimensional angle resolved scattering," Opt. Express **18**, 14616–14626 (2010).
91. H. Yu, H. Park, Y. Kim, M. W. Kim, and Y. Park, "Fourier-transform light scattering of individual colloidal clusters," Opt. Lett. **37**, 2577–2579 (2012).
92. D. J. Cuccia, F. Bevilacqua, A. J. Durkin, F. R. Ayers, and B. J. Tromberg, "Quantitation and mapping of tissue optical properties using modulated imaging," J. Biomed. Opt. **14**, 024012 (2009).
93. G. Popescu, T. Ikeda, R. R. Dasari, and M. S. Feld, "Diffraction phase microscopy for quantifying cell structure and dynamics," Opt. Lett. **31**, 775–777 (2006).
94. Y. Jo, J. H. Jung, J. W. Lee, D. Shin, H. Park, K. T. Nam, J.-H. Park, and Y. K. Park, "Angle-resolved light scattering of individual rod-shaped bacteria based on Fourier transform light scattering," Sci. Rep. **4**, 5090 (2014).
95. Y. Jo, J. Jung, M. H. Kim, H. Park, S. J. Kang, and Y. Park, "Label-free identification of individual bacteria using Fourier transform light scattering," Opt. Express **23**, 15792–15805 (2015).
96. M. Mir, T. Kim, A. Majumder, M. Xiang, R. Wang, S. C. Liu, M. U. Gillette, S. Stice, and G. Popescu, "Label-free characterization of emerging human neuronal networks," Sci. Rep. **4**, 4434 (2014).
97. J.-Y. Zheng, R. M. Pasternack, and N. N. Boustany, "Optical scatter imaging with a digital micromirror device," Opt. Express **17**, 20401–20414 (2009).
98. R. M. Pasternack, J.-Y. Zheng, and N. N. Boustany, "Optical scatter changes at the onset of apoptosis are spatially associated with mitochondria," J. Biomed. Opt. **15**, 040504 (2010).
99. H. Ding, F. Nguyen, S. A. Boppart, and G. Popescu, "Optical properties of tissues quantified by Fourier-transform light scattering," Opt. Lett. **34**, 1372–1374 (2009).
100. M. Lee, E. Lee, J. H. Jung, H. Yu, K. Kim, S. Lee, Y. Jeong, and Y. Park, "Label-free optical quantification of structural alterations in Alzheimer's disease," Sci. Rep. **6**, 31034 (2016).
101. D. J. Cuccia, F. Bevilacqua, A. J. Durkin, and B. J. Tromberg, "Modulated imaging: quantitative analysis and tomography of turbid media in the spatial-frequency domain," Opt. Lett. **30**, 1354–1356 (2005).
102. S. Gioux, A. Mazhar, B. T. Lee, S. J. Lin, A. M. Tobias, D. J. Cuccia, A. Stockdale, R. Oketokoun, Y. Ashitate, E. Kelly, M. Weinmann, N. J. Durr, L. A. Moffitt, A. J. Durkin, B. J. Tromberg, and J. V. Frangioni, "First-in-human pilot study of a spatial frequency domain oxygenation imaging system," J. Biomed. Opt. **16**, 086015 (2011).
103. A. Ponticorvo, D. M. Burmeister, B. Yang, B. Choi, R. J. Christy, and A. J. Durkin, "Quantitative assessment of graded burn wounds in a porcine model using spatial frequency domain imaging (SFDI) and laser speckle imaging (LSI)," Biomed. Opt. Express **5**, 3467–3481 (2014).
104. A. Yafi, F. K. Muakkassa, T. Pasupneti, J. Fulton, D. J. Cuccia, A. Mazhar, K. N. Blasiole, and E. N. Mostow, "Quantitative skin assessment using spatial frequency domain imaging (SFDI) in patients with or at high risk for pressure ulcers," Lasers Surg. Med. **49**, 827–834 (2017).
105. J. B. Travers, C. Poon, D. J. Rohrbach, N. M. Weir, E. Cates, F. Hager, and U. Sunar, "Noninvasive mesoscopic imaging of actinic skin damage using spatial frequency domain imaging," Biomed. Opt. Express **8**, 3045–3052 (2017).
106. D. J. Rohrbach, D. P. Muffoletto, J. Huihui, R. B. Saager, K. L. Keymel, A. D. Paquette, J. M. Morgan, N. C. Zeitouni, and U. Sunar, "Preoperative mapping of nonmelanoma skin cancer using spatial frequency domain and ultrasound imaging," Acad. Radiol. **21**, 263–270 (2014).
107. D. M. McClatchy, A. Ponticorvo, S. D. Konecky, H. Cui, T. B. Rice, B. Choi, A. J. Durkin, and B. J. Tromberg, "Light scattering measured with spatial frequency domain imaging can predict stromal versus epithelial proportions in surgically resected breast tissue," J. Biomed. Opt. **24**, 1–11 (2018).
108. A. J. Lin, M. A. Koike, K. N. Green, J. G. Kim, A. Mazhar, T. B. Rice, F. M. LaFerla, and B. J. Tromberg, "Spatial frequency domain imaging of intrinsic optical property contrast in a mouse model of Alzheimer's disease," Ann. Biomed. Eng. **39**, 1349–1357 (2011).
109. R. P. Singh-Moon, D. M. Roblyer, I. J. Bigio, and S. Joshi, "Spatial mapping of drug delivery to brain tissue using hyperspectral spatial frequency-domain imaging," J. Biomed. Opt. **19**, 96003 (2014).
110. R. H. Wilson, C. Crouzet, M. Torabzadeh, A. K. Bazrafkan, M. Hosseini-Farahabadi, B. Jamasian, D. Donga, J. Alcocer, S. M. Zaher, B. Choi, and Y. Akbari, "High-speed spatial frequency domain imaging of rat cortex detects dynamic optical and physiological properties following cardiac arrest and resuscitation," Neurophotonics **4**, 1 (2017).
111. S. C. Kanick, D. M. McClatchy, V. Krishnaswamy, J. T. Elliott, K. D. Paulsen, and B. W. Pogue, "Sub-diffusive scattering parameter maps recovered using wide-field high-frequency structured light imaging," Biomed. Opt. Express **5**, 3376–3390 (2014).
112. L. M. Almassalha, G. M. Bauer, J. E. Chandler, S. Gladstein, L. Cherkezyan, Y. Stypula-Cyrus, S. Weinberg, D. Zhang, P. T. Ruhoff, H. K. Roy, H. Subramanian, N. S. Chandel, I. Szleifer, and V. Backman, "Label-free imaging of the native, living cellular nanoarchitecture using partial-wave spectroscopic microscopy," Proc. Natl. Acad. Sci. USA **113**, E6372–E6381 (2016).
113. M. Schürmann, J. Scholze, P. Müller, J. Guck, and C. J. Chan, "Cell nuclei have lower refractive index and mass density than cytoplasm," J. Biophoton. **9**, 1068–1076 (2016).
114. A. Brunsting and P. F. Mullaney, "Differential light scattering from spherical mammalian cells," Biophys. J. **14**, 439–453 (1974).
115. R. A. Meyer and A. Brunsting, "Light scattering from nucleated biological cells," Biophys. J. **15**, 191–203 (1975).
116. Y. Sung, W. Choi, C. Fang-Yen, K. Badizadegan, R. R. Dasari, and M. S. Feld, "Optical diffraction tomography for high resolution live cell imaging," Opt. Express **17**, 266–277 (2009).
117. W. Choi, C. Fang-Yen, K. Badizadegan, S. Oh, N. Lue, R. R. Dasari, and M. S. Feld, "Tomographic phase microscopy," Nat. Methods **4**, 717–719 (2007).
118. W. J. Eldridge, Z. A. Steelman, B. Loomis, and A. Wax, "Optical phase measurements of disorder strength link microstructure to cell stiffness," Biophys. J. **112**, 692–702 (2017).
119. P. Marquet, B. Rappaz, P. J. Magistretti, E. Cuche, Y. Emery, T. Colomb, and C. Depeursinge, "Digital holographic microscopy: a noninvasive contrast imaging technique allowing quantitative visualization of living cells with subwavelength axial accuracy," Opt. Lett. **30**, 468–470 (2005).
120. M. Skacel, R. E. Petras, T. L. Gramlich, J. E. Sigel, J. E. Richter, and J. R. Goldblum, "The diagnosis of low-grade dysplasia in Barrett's esophagus and its implications for disease progression," Am. J. Gastroenterol. **95**, 3383–3387 (2000).
121. T. Benaglia, L. D. Sharples, R. C. Fitzgerald, and G. Lyratzopoulos, "Health benefits and cost effectiveness of endoscopic and nonendoscopic cytosponge screening for Barrett's esophagus," Gastroenterology **144**, 62–73.e6 (2013).
122. Z. Movasaghi, S. Rehman, and I. U. Rehman, "Raman spectroscopy of biological tissues," Appl. Spectrosc. Rev. **42**, 493–541 (2007).
123. E. Hanlon, R. Manoharan, T. W. Koo, K. E. Shafer, J. T. Motz, M. Fitzmaurice, J. R. Kramer, I. Itzkan, R. R. Dasari, and M. S. Feld, "Prospects for in vivo Raman spectroscopy," Phys. Med. Biol. **45**, R1 (2000).
124. T. C. B. Schut, T. C. Bakker Schut, F. Heule, P. J. Caspers, D. P. Hayes, M. H. Neumann, and G. J. Puppels, "Discriminating basal cell carcinoma from its surrounding tissue by Raman spectroscopy," J. Invest. Dermatol. **119**, 64–69 (2002).
125. G. Scarcelli and S. H. Yun, "Multistage VIPA etalons for high-extinction parallel Brillouin spectroscopy," Opt. Express **19**, 10913–10922 (2011).
126. A. J. Traverso, J. V. Thompson, Z. A. Steelman, Z. Meng, M. O. Scully, and V. V. Yakovlev, "Dual Raman-Brillouin microscope for chemical and mechanical characterization and imaging," Anal. Chem. **87**, 7519–7523 (2015).
127. Z. Meng, A. J. Traverso, C. W. Ballmann, M. A. Troyanova-Wood, and V. V. Yakovlev, "Seeing cells in a new light: a renaissance of Brillouin spectroscopy," Adv. Opt. Photon. **8**, 300–327 (2016).